Nb_3Sn: Macrostructure, Microstructure, and Property Comparisons for Bronze and Internal Sn Process Strands

P. J. Lee†, A. A. Squitieri and D. C. Larbalestier*
Applied Superconductivity Center, University of Wisconsin-Madison, Madison WI 53706, USA

Abstract **— The variation in irreversibility field, $B^*(T)$, with temperature has been measured for Nb_3Sn superconducting strands manufactured for ITER using vibrating sample and SQUID magnetometers. The high performance strands were developed for both high transport critical current density, J_c, and low hysteresis loss. Despite a wide variety of designs and components, the strands could be split into two distinctive groups, based on the extrapolated irreversibility fields, which lie about 10 % lower than the upper critical field. "Bronze-process" strands exhibited consistently higher $B^*(T)$ (28 T to 31 T) compared with "internal Sn" process (24 T to 26 T) conductors. The intrinsic critical current density of the superconductor, $J_{c(sc)}$, and the specific pinning force of the grain boundaries, Q_{gb}, were evaluated using the measured J_c, and image analysis of the macro- and micro- structures. A bronze-processed Nb(-Ta)$_3$Sn was found to have a higher $J_{c(sc)}$ but lower Q_{gb} than Nb_3Sn produced from Nb filaments. This work shows that the maximization of J_c is both an intrinsic flux pinning issue and a quantitative issue of how much Nb_3Sn can be put into the composite package. The results for the ITER strands are compared to a high J_c (but also high hysteresis loss) internal Sn strand. The high J_c strand had a much higher $J_{c(sc)}$ and Q_{gb} than any of the ITER strands.**

I. Introduction

The ITER program successfully produced over 28 tonnes of Nb_3Sn strand for its model coils in a development program that has pushed Nb_3Sn conductor technology to new performance and production benchmarks. The strand was successfully fabricated into 7 km of finished cable with ~1000 strands per cross-section. The strand benchmarks for ITER strand were overall critical current, I_c, and hysteresis loss, properties of the whole composite, rather than of the Nb_3Sn itself. In this note, we turn to an evaluation of the intrinsic Nb_3Sn properties such as $B^*(T)$, $J_{c(sc)}$ and Q_{gb}, deduced from magnetization and quantitative metallography.

A summary of the samples used is shown in Table I. A summary of results from the first and second ITER benchmark [1] and the third round of ITER strand bench-marking [2] are published elsewhere. The strands had been heat treated under vacuum conditions at the MIT Plasma Science and Fusion Center and the Low Temperature Division of the University of Twente, according to schedules provided by the strand manufacturers [1,2]. The heat treatments recommended by the strand manufacturers are listed in Table II.

Manuscript received September 27th, 1999.
This work supported by the US Dept. of Energy, Office of Fusion Energy Sciences, DE-FG02-86ER52131 and Division of High Energy Physics, DE-FG02-91ER40643. This work also benefited from NSF-MRSEC DMR-9632427 supported facilities.
*Also the Department of Materials Science and Engineering.
† Email: lee@engr.wisc.edu. Internet: http://www.cae.wisc.edu/~plee/

TABLE I
SUMMARY OF ITER BENCHMARK SAMPLES TESTED

Manufacturer	ITER Strand Specification	Manufacturing Technique	Reported Filament Alloy	Designation
Alsthom	HPII	Internal Sn	NA	ALS
Bochvar	HPII	Bronze	Nb + Ta Core	BOC
EM-LMI	HPI	Internal Sn	NbTi1%	LMI
Furukawa	HPII	Bronze	Nb	FUR
Hitachi	HPII	Bronze	NbTa0.5%	HIT
IGC-AS	HPI	Internal Sn	NbTa7.5%	IGC
Mitsubishi	HPII	Internal Sn	Nb	MIT
TWC	HPI	Internal Sn	NbTi1%	TWC
Vacuumschmelze	HPII	Bronze	NbTa7.5%	VAC

II. Experimental Procedure

Magnetization was measured in a laboratory constructed vibrating sample magnetometer (VSM), which was used to observe the DC moment as a superconducting solenoid swept the field from 0 T to 12 T and back at 20 mT per second. These field sweeps were taken at 4.5 K and every 0.5 K from 8 K to 14 K, with some samples also tested at 15 K and 16 K. Sample temperature was established at zero field by a germanium sensor in close proximity to the sample and controlled during the measurement by an adjacent capacitance sensor during the sweep. The temperature controller was an Oxford ITC-4 whose capacitance sensor board had been modified in order to greatly increase its resolution, while reducing noise and drift. Combined with a LakeShore CS-401 capacitance thermometer, this sensor and amplifier provide a sensitivity of 1 mK and intrinsic noise of < 2 mK in the 4 K - 20 K temperature range. Initial set-point deviation from the nominal temperature was ≤ 0.02 K, and control stability during sweeps was 0.01 K. Temperature offsets due to spatial separation of the thermometers and the sample

TABLE II
RECOMMENDED HEAT TREATMENT SUPPLIED BY MANUFACTURERS

Strand	Recommended Heat Treatment
Bochvar	575° C/150 h, 650° C/200 h
EM-LMI	220° C/175 h, 340° C/ 96 h, 650° C/180 h
Furukawa	650° C/240 h
Hitachi	650° C/200 h
IGC-AS	660° C/240 h, (6° /h ramp)
Mitsubishi	200° C/6 h, 350° C/18 h, 450° C/28 h, 580° C/60 h, 700° C/160 h
TWC	185° C/120 h, 340° C/72 h, 650° C/200 h
VAC	570° C/220 h, 650° C/175 h

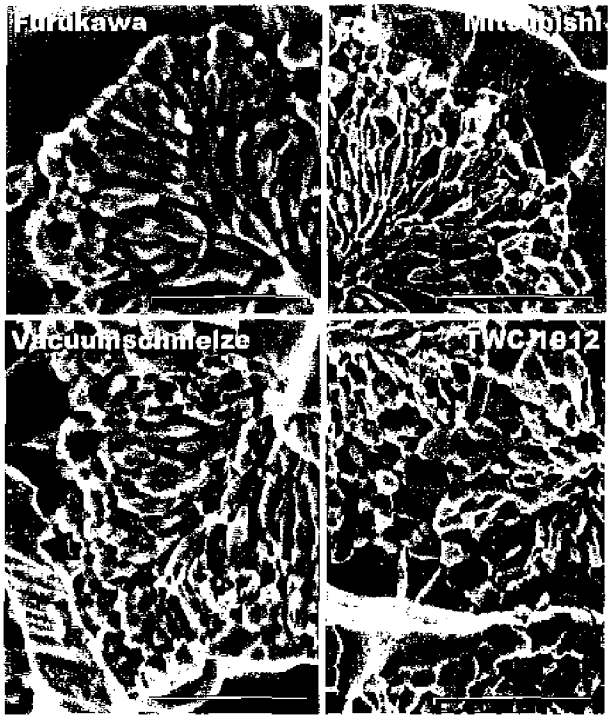

Fig. 1. FESEM-SE images of fracture cross-sections comparing the Nb_3Sn grain size from filaments of the Furukawa, Mitsubishi and Vacuumschmelze ITER strands as well as the high J_c TWC (1912) strand. The magnifications are the same and the scale markers are 1 μm in length.

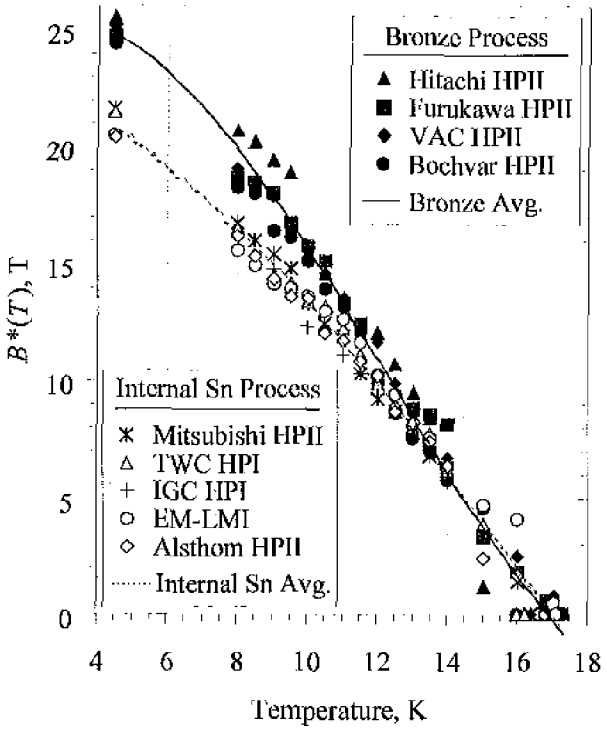

Fig. 2. Variation in irreversibility field, $B^*(T)$ with temperature for ITER 2nd and 3rd benchmark strands. Note the separation between bronze-process and internal tin processed strand.

were nulled by measuring $T_{c(0)}$ of a sample of Nb. Control set-point stability of the capacitor was verified by controlling sample temperature at zero field with the capacitor, while monitoring the sample temperature with the control germanium thermometer. The temperature control tests spanned 60 minutes, a period double the time of one field sweep. A few samples were also measured in a Quantum Design MPMS-5 magnetometer at 16 K, which was also used to measure T_c in a field of 5 mT. Total temperature error in the SQUID was 0.02 K. The irreversibility field [3], B^*, values for each temperature, $B^*(T)$, were estimated from straight-line extrapolations of magnetization data converted to Kramer plots, $J_c^{1/2}B^{1/4}$ (B,T).

The $J_{c(sc)}$ was obtained from the previously reported transport I_c values [2], dividing I_c by the measured cross-sectional area of the Nb_3Sn A-15 phase, rather than as usual by the overall diffusion barrier, bronze, Sn, etc package needed to make the Nb_3Sn. Areas were determined by image analysis of back-scattered electron images obtained in a LEO 982 FESEM. The Q_{gb} was obtained from the $J_{c(sc)}$ data by measuring the grain boundary density from high resolution secondary electron images of fracture cross-sections (Fig. 1) by a previously reported method [4]. Low magnification sampling of large areas was checked against high magnification images of small numbers of filaments.

III. Results

The $B^*(T)$ results (Fig. 2) show a striking result, namely that the internal tin and the bronze composites have divergent trends, in general agreement with the trends of Kramer plots for J_c data. Above 5 T there is a distinct separation between internal Sn and bronze-processed strands, bronze strands having higher $B^*(T)$.

The $J_{c(sc)}$ (Fig. 3) and Q_{gb} results (Fig. 4) indicate a lower $J_{c(sc)}$ for the bronze strand and a lower grain boundary pinning force. The high J_c high Sn comparison strand has a substantially higher $J_{c(sc)}$ and Q_{gb} than the ITER strands.

The distribution of grain sizes (expressed here as d^*, the diameter of the grains calculated from their cross-sectional areas, assuming circular cross-sections) within the filaments was log-normal for all the strands studied. The grain size and size distribution was typically uniform from filament to filament with some exceptions. For the Furukawa bronze-processed strand, the grain size for the filaments closest to the outside of the filament pack (F1 and F2 in Fig. 5) are 25 % greater than for the interior of the filament pack. The grain size distributions for the bronze-process Furukawa strand are shown in (Fig. 5) and can be contrasted with the more uniform grain size distributions for 3 filaments from the internal Sn processed Europa Metalli LMI strand. This was not a universal trend for internal Sn strands as cross-

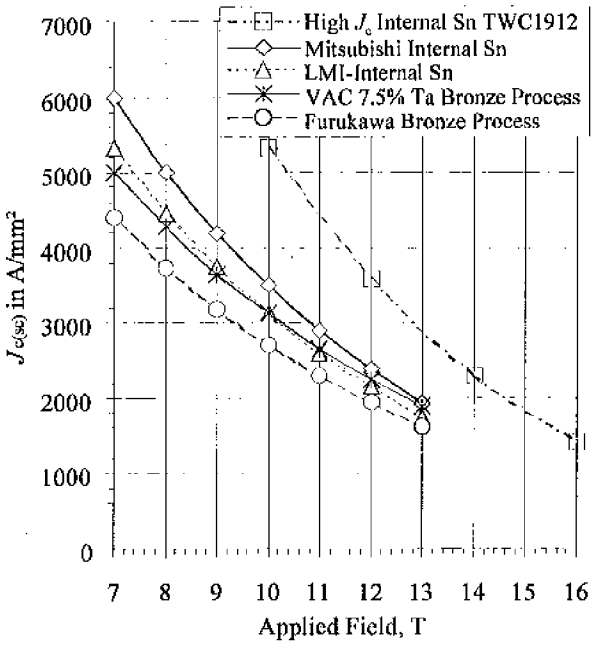

Fig. 3. Variation in superconductor critical current, $J_{c(sc)}$ with applied field. The internal Sn process strands have a higher $J_{c(sc)}$, especially the high Sn strand. For the Vacuumschmelze 7.5 % Ta strand, the decrease in $J_{c(sc)}$ with field is less at high field than the internal Sn strands, resulting in a cross-over with the Europa Metalli-LMI internal Sn strand at 10 T.

sub-element trends in filament size were also observed for the Mitsubishi internal Sn strand.

A trend to reduced grain boundary density with increasing

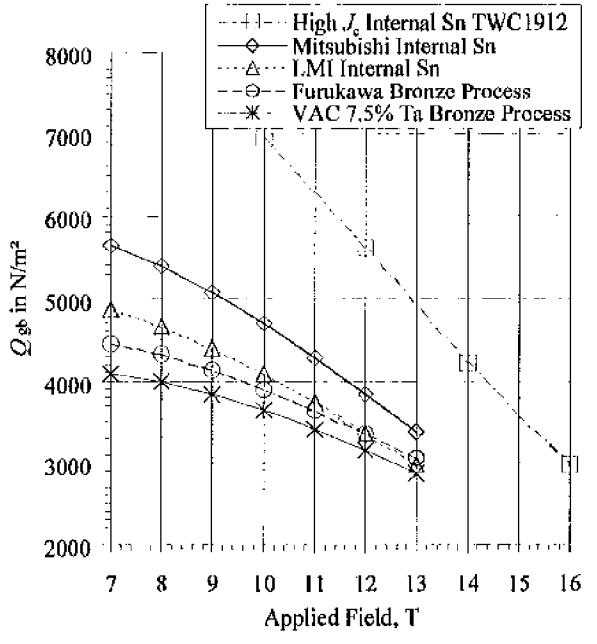

Fig. 4. Variation in grain boundary specific pinning force, Q_{gb}, with applied field. The high Sn internal Sn strand has almost double the Q_{gb} of the other strands. Even the low Sn ITER internal Sn strands have a higher Q_{gb} than the bronze-processed strands. The high grain boundary density of the Vacuumschmelze bronze strand (7.5 %Ta) lowers the calculated Q_{gb} significantly below that of the Furukawa bronze-processed strand.

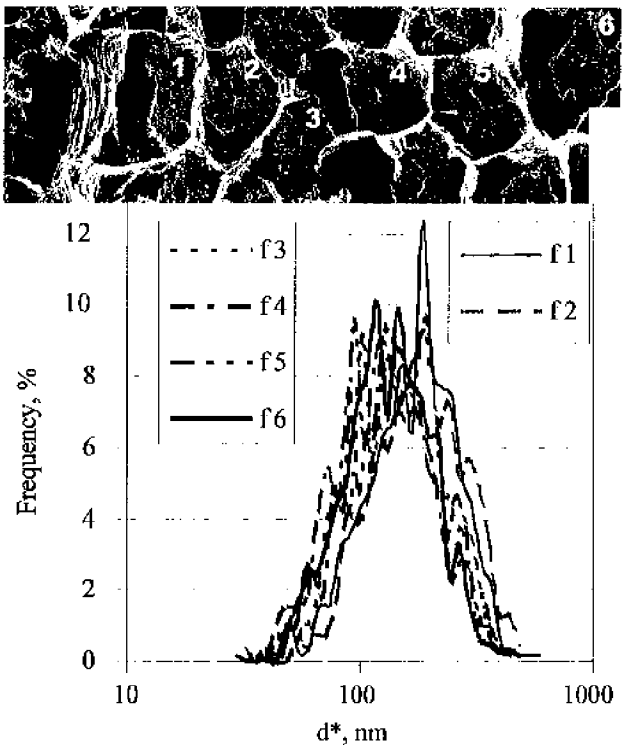

Fig. 5. Variation in grain size with location for Furukawa bronze-processed ITER strand. The grain size for the filaments closest to the outside of the filament pack (F1 and F2) are 25% greater than for the interior of the filament pack. The coefficient of variation for d^* for the 6 filaments, is a relatively large 13 %; the mean grain size (log) was 146 nm with a +1 std. dev. of 84 nm.

distance from the original reaction interface (filament perimeter) is observed in the Furukawa strand (i.e. Fig. 7) with a gradient of approximately $-4E^{-06}$ nm^{-2}. This trend was also observed in the Vacuumschmelze bronze-processed strand ($-3E^{-06}$ nm^{-2}). The trend was very shallow in the LMI strand ($-7E^{-7}$ nm^{-2}) and in the Mitsubishi strand the trend was reversed and the grain boundary density increased with increasing distance from the perimeter of the filament ($+3E^{-06}$ nm^{-2}). The reduction in grain boundary density occurs simultaneously with an increase in the aspect ratio of the grains, as the grains become more columnar towards the center of the filament. Columnar grain growth occurs when new grains are not nucleated and while the Nb_3Sn grains continue to grow inward and are restricted in their perpendicular growth by adjacent grains.

IV. Discussion

The finding that bronze ITER strands have intrinsically better $B^*(T)$ properties than ITER internal Sn strands was not at all expected, as higher J_c and presumed better intrinsic properties are normally thought to occur in internal Sn conductors. This distinction occurred despite a large number of other design variables (see Table I). The implication is that whatever benefit the ITER internal Sn conductors derive because of their smaller "carrier" Cu content, is at least

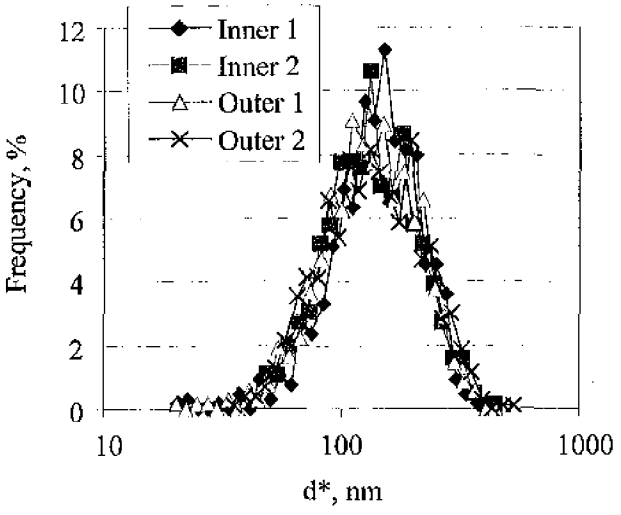

Fig. 6. Variation in grain size (d^*) with position for four filaments in the Europa Metalli LMI strand, comparing outer and inner filaments. The grain size is uniform with a coefficient of variation of just 3 %. The mean grain size (log) was 134 nm with a +1 std. dev. of 77 nm.

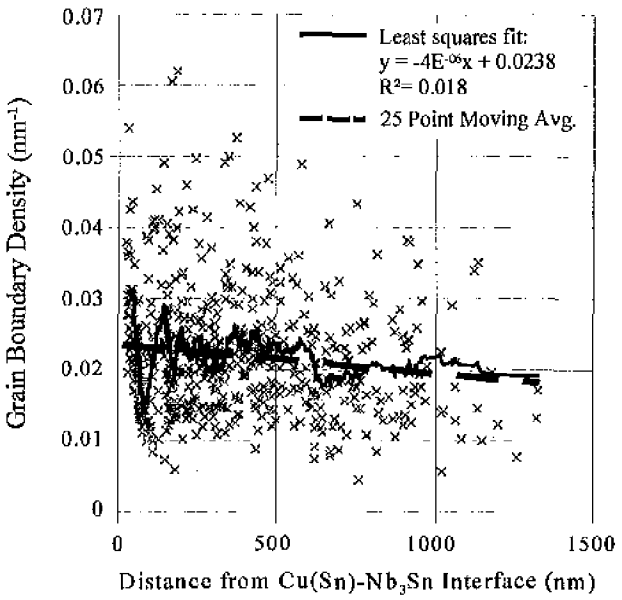

Fig. 7. Variation in grain boundary density with position within an inner filament of the Furukawa bronze strand (filament 6 of Fig. 5). A 25 point moving average is shown as a continuous black line. The least squares linear fit (dashed line) shows a reasonable approximation to the trend.

partially negated by their inferior basic Nb_3Sn properties. This result is also striking because bronze conductors with larger "carrier" Cu content might be expected to have greater pre-compression and thus depressed T_c, B_{c2} and $B^*(T)$. The unexpected behavior of the internal Sn composites may be due to the design compromises that had to be made in order to reduce the hysteresis loss of the internal Sn strands. Despite the superior $T_c(B)$ behavior of the bronze strands, the $J_{c(sc)}$ and Q_{gb} of the two bronze strands were lower than internal Sn strands.

The difference between the Q_{gb} of the Furukawa bronze and the Vacuumschmelze bronze-processed strand is also interesting. The principal difference between the Vacuumschmelze strand and the Furukawa strand is the use of 7.5 wt. % Ta alloy Nb filaments in the case of the Vacuumschmelze strand. The use of Ta has long been known to improve high field performance, and it has been postulated that this is a result of increased critical fields produced by a decreased electron mean free path [5]. In this case, however, the increased grain boundary density that should result in significantly higher critical current is apparently offset by a reduced pinning force supplied by the grain boundaries.

We first reported the log-normal distribution of Nb_3Sn grain size for an early TWC ITER strand [4]. By accurately describing the distribution profile, meaningful statistics can be generated for filament size distributions. Having confidence in the measurement statistics, we can now search for trends in the variation of d* distributions.

For bronze-processed strand, unlike internal Sn, the Sn is uniformly distributed across the bronze prior to the onset of the Nb_3Sn strand. This situation, however, can be expected to change as Sn is depleted from the bronze. We have recently observed a variation in grain size with location for Vacuumschmelze (13.5 % Sn) bronze-processed strand [6] and in this case a larger grain size was observed for filaments nearest the outside of the strand. Further study of this phenomenon should yield insights as to how to increase grain boundary density.

ACKNOWLEDGMENTS

We thank Milan Polak and Makoto Takayasu (MIT) for their help in this work. The high J_c internal Sn strand was courtesy of Oremet Wah Chang, formerly Teledyne Wah Chang Albany.

REFERENCES

[1]P. Bruzzone, H.H. ten Kate, M. Nishi, A. Shikov, J. Minervini, M. Takayasu, "Bench Mark testing of Nb3Sn strands for the ITER model coils", Adv. in Cryo. Eng. Plenum Press, NY, Vol. 42B, ed. L. Summers pp. 1351-1358, 1997.

[2]Hennie G. Knoopers, Arend Nijhuis, Erik J.G. Krooshoop, Herman H.J. ten Kate, Pierluigi Bruzzone, Peter J. Lee and Alexander A. Squitieri, "Third Round of the ITER Nb_3Sn Strand Bench Mark Test," "Applied Superconductivity 1997, edited by D H A Blank, and H Rogalla, University of Twente, The Netherlands, pp. 1271-1274, 1997.

[3]M. Suenaga, A. K. Ghosh, Xu Youwen, D. O. Welch, "Irreversibility temperatures of Nb_3Sn and Nb-Ti," Phys. Rev. Let., vol. 66, no.13, pp.1777-80, 1 April 1991.

[4]P. J. Lee, J. R. Ruess and D. C. Larbalestier, "Quantitative Image Analysis of Filament Coupling and Grain Size in ITER $Nb(Ti)_3Sn$ Strand Manufactured by the Internal Sn Process," IEEE Trans. Applied Superconductivity, vol. 7(2), pp. 1516-1519, 1997.

[5] J. D. Livingston, "Effect of Ta additions to bronze-processed Nb_3Sn superconductors," IEEE Trans. Mag., vol 14, no.5, pp.611-13, Sept. 1978.

[6] R. Kimmich and P. Lee, "Microstructure of Commercial Nb_3Sn-Composites," internal report for Forschungszentrum Karlsruhe, Institut fuer Technische Physik, 1999.